IET Microwaves, Antennas & Propagation

vol. 10, no. 13, pp. 1411-1419, 10 22 2016.
doi: 10.1049/iet-map.2016.0013
http://ieeexplore.ieee.org/stamp/stamp.jsp?tp=&arnumber=7637125&isnumber=7637099

3D-Printed Planar Graded Index Lens

Shiyu Zhang [*1], Ravi Kumar Arya [2], Shaileshchandra Pandey [2], Yiannis Vardaxoglou [1], Will Whittow [1], Raj Mittra [3]

[1] Wolfson School of Mechanical, Electrical and Manufacturing Engineering, Loughborough University, Loughborough, Leicestershire, LE11 3TU, United Kingdom
[2] EMC Lab, Pennsylvania State University, University Park, PA, USA
[3] EMC Laboratory, University of Central Florida, Florida, United States of America & EE Department, KAU, Saudi Arabia
[*] s.zhang@lboro.ac.uk

Abstract: We introduce two flat graded-index (GRIN) lens designs in this paper. First of these is a thick lens which was designed and fabricated by using the 3D-printing technique. Second, a thin Dial-a-Dielectric (DaD) lens which uses state-of-the-art artificially engineered dielectric materials for design and will be fabricated in future. Both designs overcome the difficulties faced in finding desired commercial off-the-shelf (COTS) materials for 3D-printing lenses. The lenses comprise of several concentric dielectric rings with bespoke relative permittivities for transforming spherical waves into plane waves and vice versa. The 3D-printed thick flat lens is low-cost and light-weight, but provides broadband and high gain performance. Measurement results show that the realized gain of the thick lens is 9-11 dB over the frequency band of 12-18 GHz. The designed DaD lens has the desirable characteristics of low loss, low reflection and broadband properties.

1. Introduction

A lens is a well-known antenna component designed to transform a plane wave into spherical wave for focusing optical rays to a single point. It also converts the spherical wavefronts emanating from a feed, located at the focal point, into planar wavefronts; and, therefore, it can be used for antenna application to realise a high directive beam. Lenses can improve antennas by realising wide angle scanning, beamforming and enhanced gain. Furthermore, lenses generally provide broadband advantages over the conventional antenna arrays. However, classical lenses are not attractive for antenna applications due to their convex or spherical shapes. A flat lens has a low-profile, is light-weight and can be easily used in proximity to the antenna. In recent years, research into a variety of flat lens antennas has been carried out based on field transformation [1]–[3], transformation optics [4]–[6], ray optics [7] and transmit array approaches [8].

For manipulating the propagation of the electromagnetic (EM) waves, these lenses are generally designed with radially varying refractive indices that are challenging to realise and fabricate. For practical fabrication, the lenses are often comprised of several tight-fitted zones with different EM properties. However, it is difficult to source the materials in commercially off-the-shelf form that have the required EM properties. Another method to produce tailored EM properties is by perforating a homogeneous slab

with variable hole diameters or separations [9]. Precise machining and tight tolerances are required in this approach, particularly for high frequency applications. Sometimes the maximum number of holes is limited to prevent the material from physically cracking. On the other hand, there are a number of methodologies which have been investigated for tailoring the EM properties by using synthetic materials [10]–[16]. The main approach of fabricating these materials for flat lenses has been based on metamaterials [17]–[20]. However, some of the metamaterial lenses suffer from narrow bandwidth, losses and dispersion. Moreover, the fabrication processes of the metamaterials based lenses are cumbersome at best.

This paper presents two novel wideband flat graded-index (GRIN) lenses with a practical fabrication approach using 3D-printing. One of the lens (thick lens) has already been fabricated while the other, namely the DaD lens can also be fabricated using the same 3D-printing strategy. 3D-printing is an additive manufacturing technique which creates 3D-objects in successive layers. It provides a practical fabrication approach to produce highly customisable structures with the advantages of low-cost and fast automated repeatable design and manufacturing. The 3D-printing process allows creating embedded sub-millimetre internal structures such as air voids in the 3D-object in a single process without machining. 3D-printed dielectric substrates with different relative permittivities ε_r was reported in [21]. Compared with perforating a solid material, the design can be easily modified and rapidly prototyped in-house by using low-cost 3D-printing materials, and this is particularly useful for building laboratory prototypes. The equation for tailoring the ε_{reff} was extrapolated from the measured results. Then the design principle of the flat lens with radially varying ε_{reff} was investigated and simulated by using CST Microwave Studio software. The entire thick GRIN lens was then fabricated with varying ε_r in a one-step process using the 3D-printing. We also measured its far-field performance using an azimuth-plane scanning system. On the other hand, DaD lens was simulated in HFSS and its behavior studied and compared with thick lens. 3D-printing is low-cost technique and enables fast automated repeatable design and manufacturing. By current trends, 3D-printing is getting accessible and affordable day-by-day and will bring the cost of such designs even lower.

2. Thick Lens Design

In this work, thermoplastic polylactic acid (PLA) was used as the print material. The Nicolson-Ross and Weir (NRW) method [22] was used to measure the ε_{reff} of the 3D-printed samples with different internal air void volumes. The PLA volume percentage (v) indicated the ratio of the volume of PLA in the printed structure to the volume of the whole structure. Measurement results from NRW indicated that the

100% infilled PLA sample had ε_r of 2.72 and the ε_r was reduced to 1.30 with the 10.1% PLA volume percentage. The measured ε_r of 3D-printed samples with different PLA volume percentages *v* showed that the relation between the ε_r and *v* was approximately linear. The expression of the required PLA volume percentage *v* for tailoring the effective permittivity ε_{reff} of the 3D-printed dielectrics was extrapolated and given by equation (1):

$$v = \frac{\varepsilon_{reff} - 1}{\varepsilon_{ro} - 1} \tag{1}$$

where ε_{ro} is the relative permittivity of the 100% PLA 3D-printing material (ε_{ro} = 2.72). The minimum ε_{rmin} is limited by the 3D-printer resolution and the total volume of the structure. Generally, high resolution printers with small diameter nozzles or structures with larger total volumes can achieve a lower ε_{reff}. This equation will be used for tailoring the effective permittivity of the 3D-printed GRIN lens in Section 3.

The thick flat GRIN lens is in the form of a disk and its focal point is located at its axis of symmetry (see Fig. 1). The refractive index should be a maximum at the centre of the lens and gradually decrease to the outermost region [23]. The required variation in the refractive index can be calculated by equating the phase delay of the rays from the focal point until where they exit the lens. It is assumed that the angle between the path where the ray enters the lens and the lens axis is θ (see Fig. 1). The relation between the radially varied ε_r and θ is given by equation (2), and this becomes the basic design equation for the thick flat GRIN lens.

$$\frac{T}{F}\left(\varepsilon_r - \frac{2}{3}\sin^2\theta\right) = \sqrt{(\varepsilon_r - \sin^2\theta)}\left(\sqrt{\varepsilon_{rmax}}\frac{T}{F} - \sec\theta + 1\right) \tag{2}$$

where *T* is the thickness of the lens, *F* is the focal length and ε_{rmax} is the maximum permittivity at the centre of the lens.

The design can be simplified by calculating ε_r for several given values of θ and then producing a smooth curve through the plotted points. Due to the limited resolution of the 3D-printer and for practical fabrication, it was considered reasonable to approximate the ideal smooth variation with a step function. Thus the lens can be fabricated from a series of concentric dielectric cylindrical rings with different relative permittivities. The design principle is shown in Fig. 1. The corresponding ε_r values for each ring was designed to enable them to have the same focal point *O* to convert the spherical wave, emanating from the focal point into a plane wave.

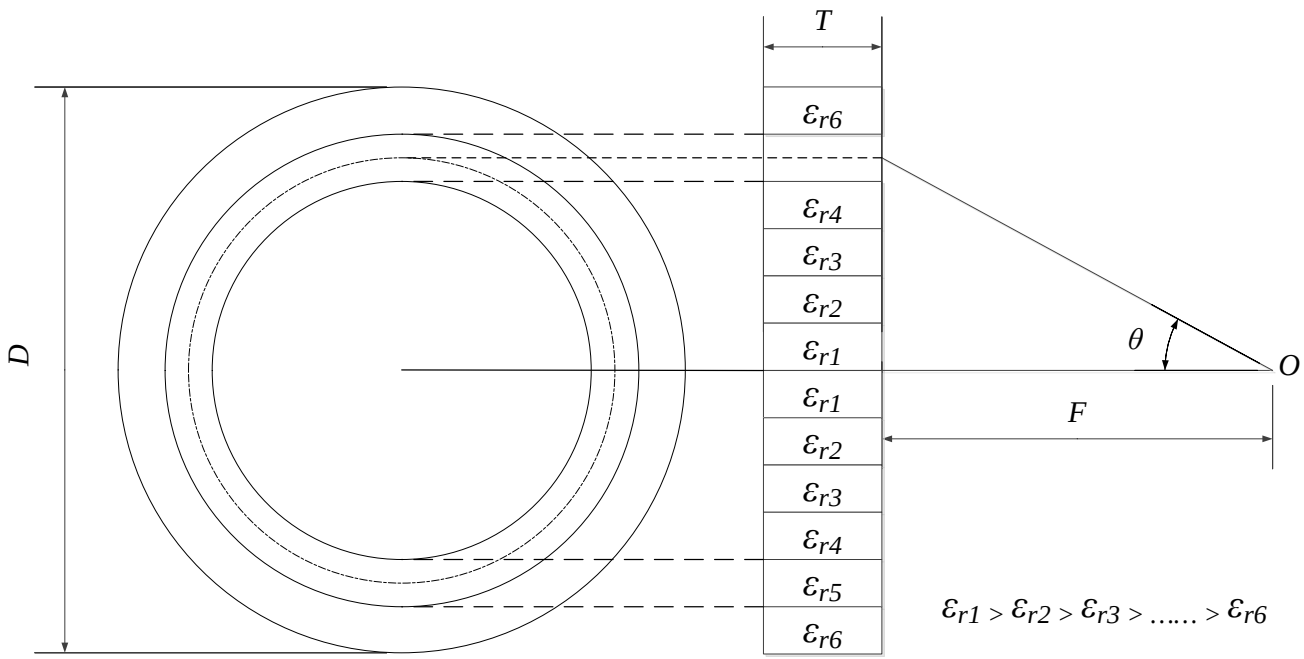

Fig. 1. *Sketch of lens design principle*

Before equation (2) can be applied to the lens design, it is necessary to know the maximum value of θ_{max} which is determined by the diameter of the lens and the focal length. In addition, knowing the minimum value ε_{rmin} which can be produced by 3D-printing is equally essential. Structural considerations limit the minimum value of ε_r due to the resolution of the 3D-printer. Having determined the values of the θ_{max} and ε_{rmin}, equation (2) was solved to find the lens thickness *T* hence the ε_r variation. The θ was measured to the centre line of the cylindrical ring as shown in Fig. 1. Equation (2) could be applied to find the focal length *F* for each cylindrical ring.

The final design parameters are shown in Table 1. The fabricated lens is comprised of six 10 mm wide discrete dielectric concentric cylindrical rings. The size of the lens is limited by the maximum printing volume (length × width × height) of the 3D-printer (24.6 cm × 15.2 cm × 15.5 cm). A larger lens could be realised by: i) using a 3D-printer which has a larger printing volume; or ii) printing multiple parts of the lens (for instance, four quarter circles) and then assembling them together. The outermost ring has the lowest effective permittivity of 1.3, while the centre ring has the highest effective permittivity of 2.72. Fig. 2 shows the step function of the variation ε_{reff} versus radial distance across the lens. In order to obtain the bespoke ε_{reff}, the air volume fraction is increased from the centre to the outermost region by decreasing the PLA volume fraction. Increasing the number of rings for a smoother permittivity variation would improve the accuracy of the focal point and increase the gain of the lens. However, narrow rings

with small variations of volume fractions are difficult to fabricate accurately due to the resolution of this printer.

Table 1 Designed parameters of 3D-printed lens

Parameter	Value
Diameter	D = 120.0 mm
Focal length	F = 150.0 mm
Thickness	T = 18.5 mm

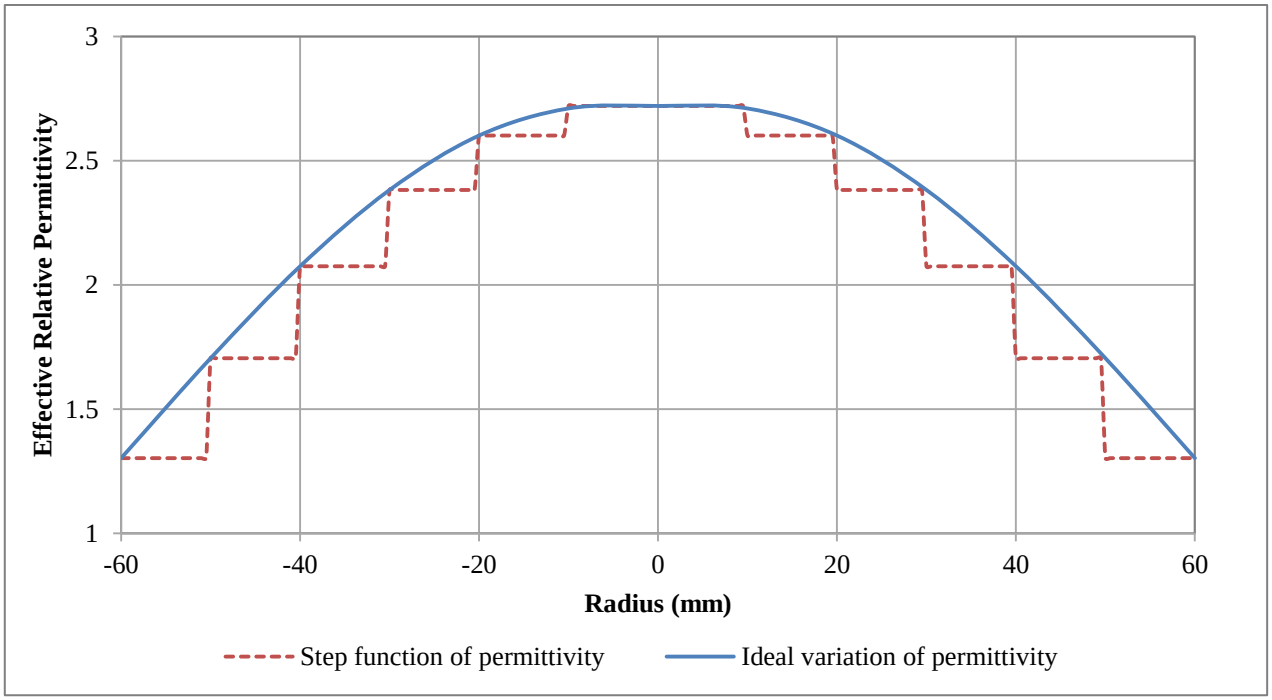

Fig. 2. *Curves of effective relative permittivity for the 3D-printed lens as a function of its radius*

A full-wave simulation using CST was carried to verify the lens design. For simplifying the simulation and reducing the computational complexity, the thick flat GRIN lens was modelled as six solid concentric cylindrical rings and the internal structures was not considered. Each ring had homogenous dielectric constant and the value of the ε_r decreased from the centre to the outermost ring as in Fig. 2. The dielectric loss tangents for all the cylinder rings were $tan\delta$ = 0.008 which was the loss tangent of 100% PLA material. Generally, lower PLA volume percentages resulted in lower loss tangent values and the decrease was approximately linear [21]. In reality the 3D-printed cylinderical rings would have lower loss

tangent values than the simulation, however, as PLA is a low-loss material, the changes were not significant.

A Ku-band conical feed horn was placed at the focal point, 150 mm away from the lens. The simulated electric field of the lens antenna at 12, 15 and 18 GHz is shown in Fig. 3. It clearly shows that the spherical wavefronts generated from the horn are converted into plane waves in the near-field region by the flat GRIN lens, and the lens results in a highly directive radiation in the far-field region. The simulated far-field directivity radiation patterns are shown in Fig. 4. A high-directivity beam in the far-field pattern in the *z* direction was observed. The gain of the thick lens antenna and the feed horn composite was 18.0, 21.4 and 24.0 dBi at 12, 15 and 18 GHz respectively. This thick lens was fabricated as discussed in Section 3.

Further simulation-only studies have been carried out to explore more complex geometries that potentially could be manufactured using a higher resolution 3D-printer. A lens with a smoother permittivity variation which was comprised of fifteen 4 mm wide rings was simulated and the gain was increased by 0.3 to 0.7 dB over the frequency range. Furthermore, a quarter wavelength thickness matching layer can be used to further improve the lens performance by reducing the reflections when the wave travels between the air and the material [24]. This is particularly useful for the GRIN lens that has the highest permittivity at the centre of the lens. In this work, the highest permittivity at the centre of the lens was 2.72 which is relatively low compared with most conventional dielectric slabs, therefore, the matching layer is less critical than when using a higher permittivity material. The simulation results showed that adding a matching layer (ε_r = 1.65) on both sides of the lens could increase the gain by up to 0.6 dB at the cost of increasing the total thickness by 7.8 mm. The advantage of using 3D-printing is that it would allow fabricating the matching layers and the lens in a single process.

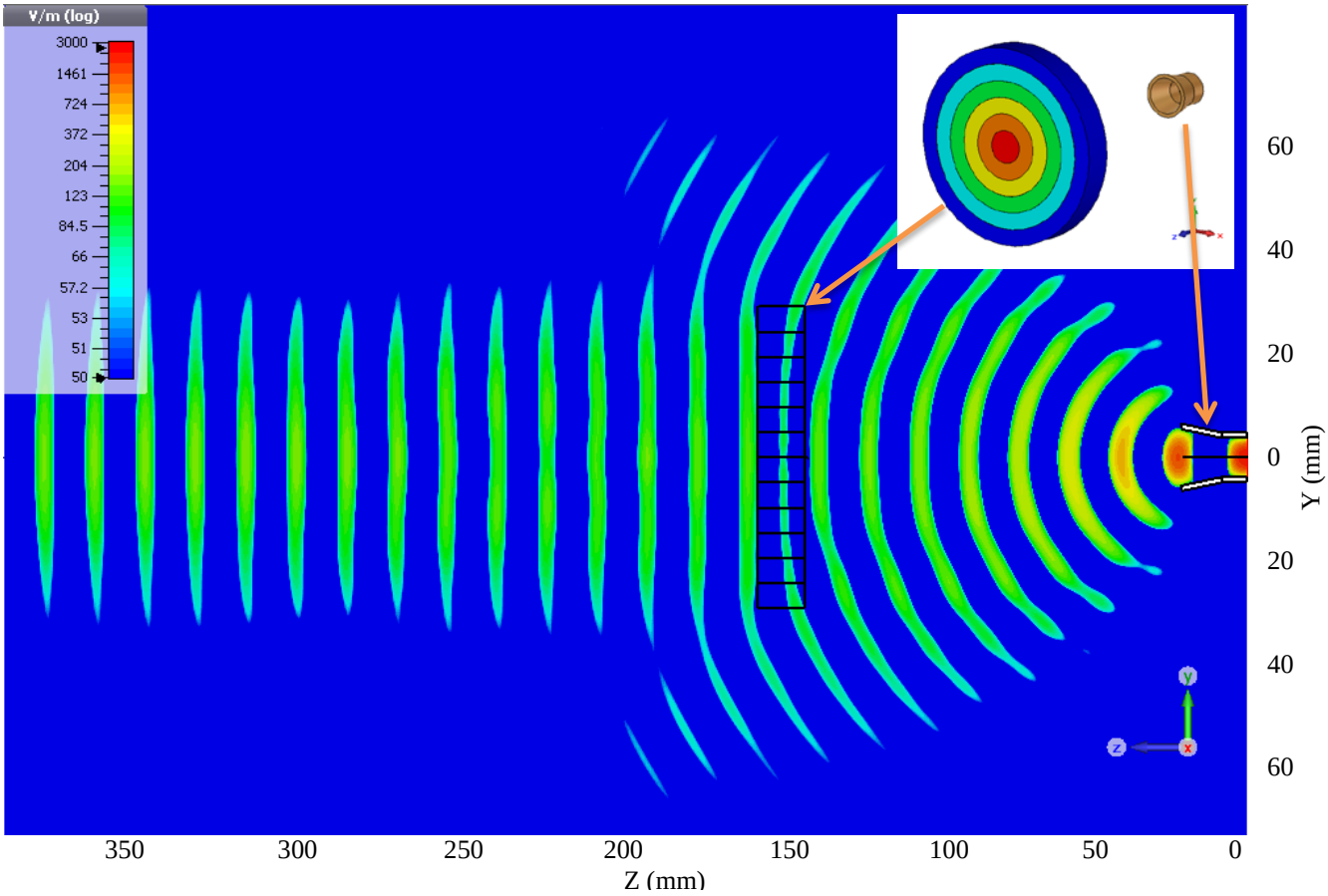

Fig. 3. *Simulated electric field of the thick flat GRIN lens at 15 GHz, fed by a circular Ku-band horn located at the focal point*

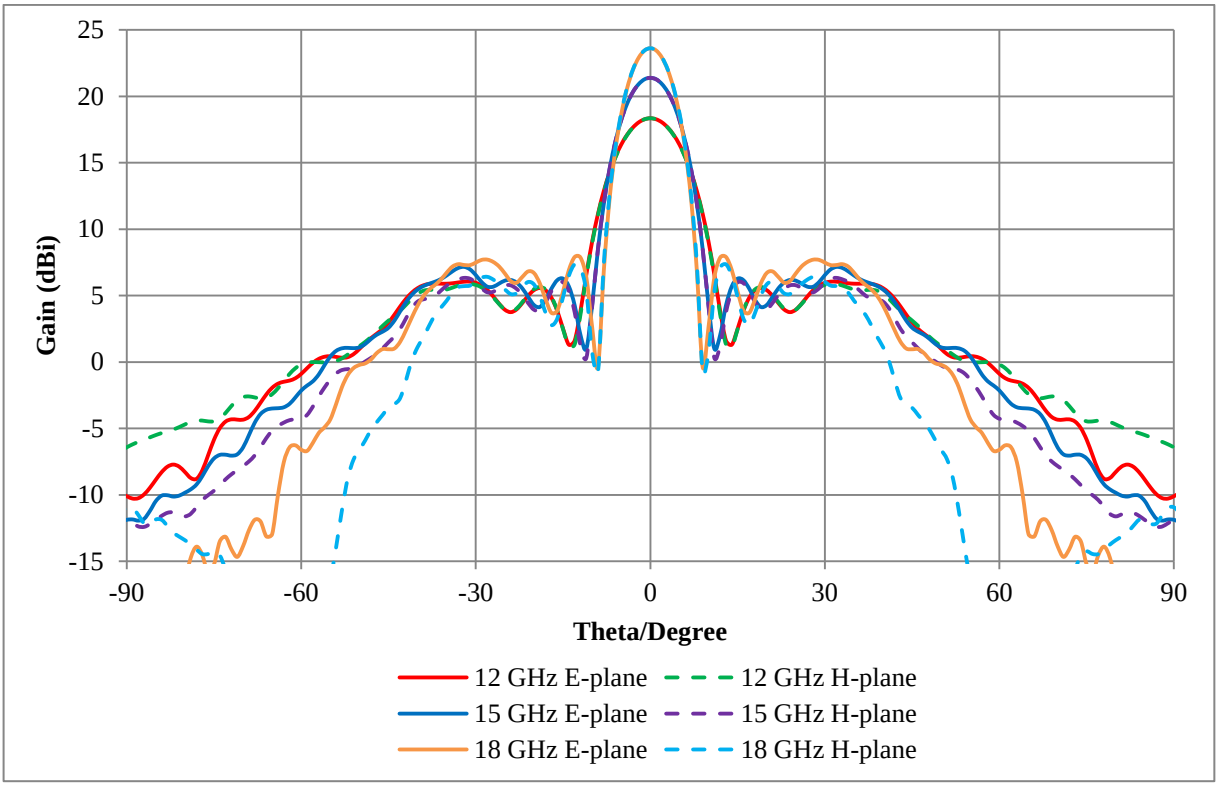

Fig. 4. *Simulated far-field gain pattern of the thick flat GRIN lens at 12, 15 and 18 GHz*

3. Thick Lens Fabrication

A Makerbot® Replicator™ 2X 3D-printer was used to fabricate the thick flat GRIN lens. This 3D-printer uses the fused deposition modelling (FDM) method which has a heated printer nozzle, extruded the thermoplastic material and created the lens layer by layer from the bottom up. The geometry of the lens in CST was exported as a Stereolithography (STL) format and then imported into 3D-printing computer aided design (CAD) software for locally changing the infill percentages to tailor the permittivities accordingly.

The 3D-printed flat lens with six different PLA volume percentages *v* in the concentric cylindrical rings is shown in Fig. 5. The matching layer was not printed in order to minimise the thickness of the lens. Equation (1) was used to determine the required *v* for each bespoke ε_r. It is worth noting that conventional desktop FDM 3D-printers use "infill density (or infill percentage)" to describe the volume fraction of the thermoplastic to the total volume but excluding the exterior walls of the 3D-object. Generally the minimum wall thickness is equal to the nozzle diameter of the 3D-printer. Therefore, the "infill density" for the 3D-printing CAD software should always be smaller than the PLA volume percentages *v* that was obtained from equation (1). In this work, the infill density *d* for each cylindrical ring can be determined by using equation (3).

$$d = \frac{v\pi\left(R^2 - r^2\right) - 2\pi t(R+r)}{\pi(R^2 - r^2) - 2\pi t(R+r)} \tag{3}$$

where *v* is the PLA volume percentage obtained from equation (1) and *t* is the exterior wall thickness. *R* and *r* are the exterior and interior radius of the cylindrical ring respectively and they include the wall thickness *t*. The Replicator 2X 3D-printer had a minimum wall thickness of 0.4 mm.

In this case, the maximum infill density at the centre was 100% and the minimum infill density of the outermost ring was 10.1%. The detailed parameters for each ring are shown in Table 2. Finally the entire thick flat GRIN lens was 3D-printed with varying ε_r in a one-step process. The 3D-printed lens had reasonable physical rigidity to resist deformation or deflection.

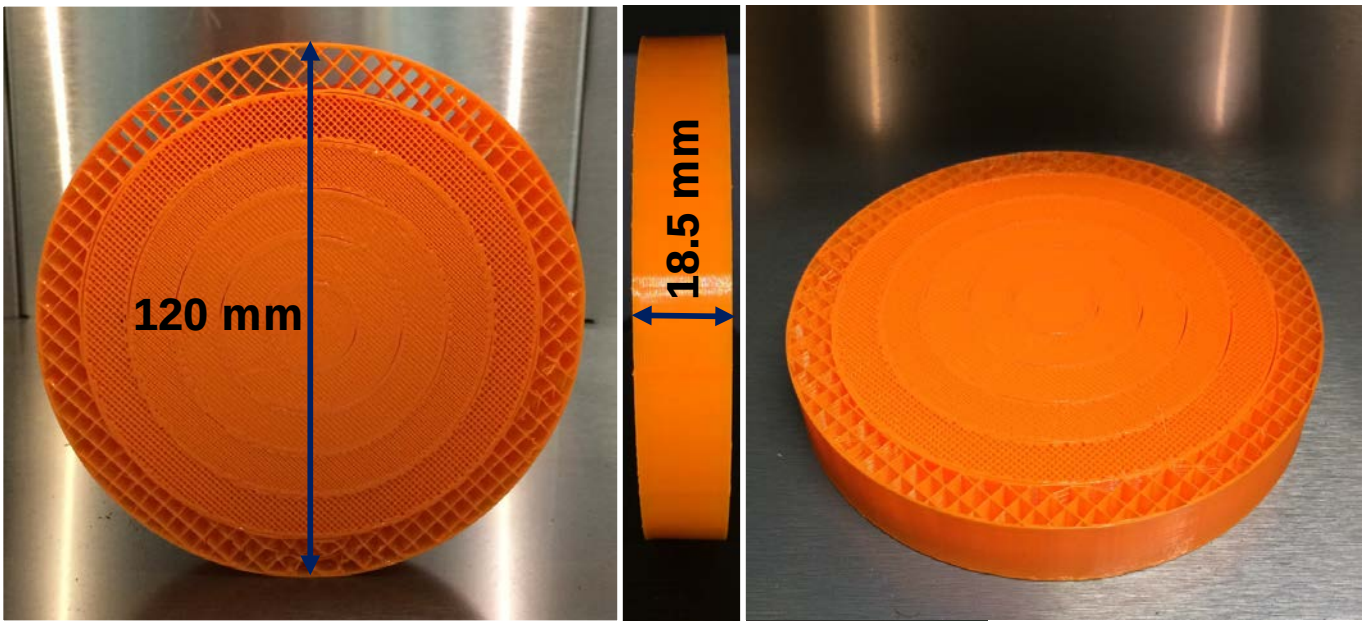

Fig. 5. *3D-printed thick flat lens*

Table 2 Parameters of 3D-printed concentric dielectric rings

Ring No.	ε_r	d
1	2.72	100%
2	2.60	90.8%
3	2.38	77.2%
4	2.08	58.0%
5	1.71	35.1%
6	1.30	10.1%

4. Thick Lens Measurements

A 180° azimuth-plane scan measurement was set up for testing of the performance of the thick 3D-printed lens. A Ku-band pyramid waveguide horn antenna, which was placed at a distance of 1.5 m along the lens axis, served as the receiving antenna. This receiving horn was freely moved from theta = -90° to theta = +90° for azimuth-plane scanning. The sketch of the azimuth scanning system is shown in Fig. 6. Note, the 1.5 m distance was slightly shorter than the far-field distance ($2D^2/\lambda$) of the lens antenna above 15.6 GHz due to the limited indoor space. A conical feed horn (open end diameter of 22.75 mm) was used

as the source to generate spherical wavefronts (see Fig. 7(a)). The 3D-printed lens was held by a foam and was perpendicular to the azimuth-plane. The feed horn was mounted on a slider at the focal point of the lens axis, which was 150 mm away from the 3D-printed lens. The feed horn can be moved along two directions in the azimuth-plane by rotating the knobs for examining the off focal point performance. The slider with the amounted feed horn is shown in Fig. 7.b.

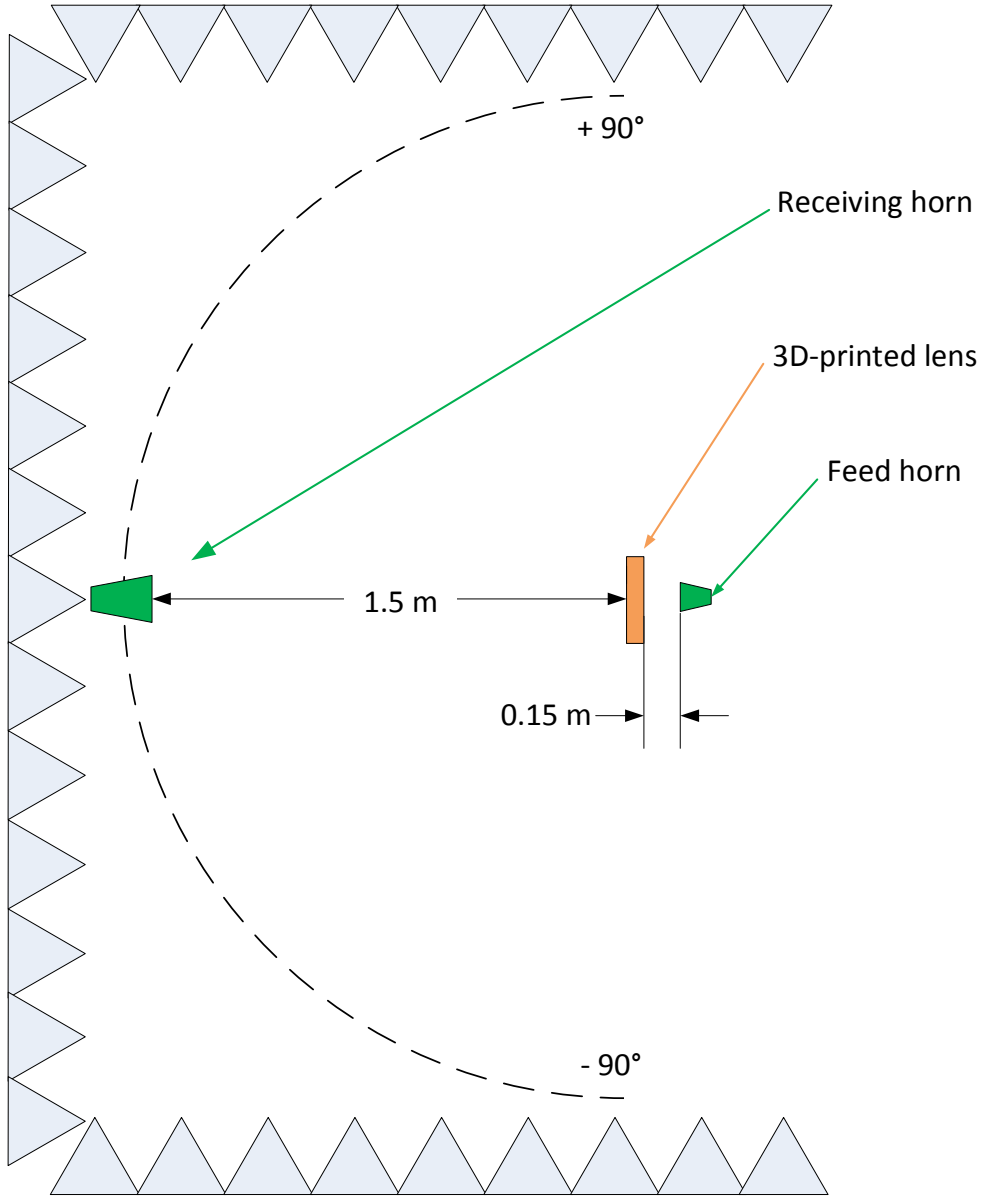

Fig. 6. *Sketch of the measurement setup for the 3D-printed lens antenna*

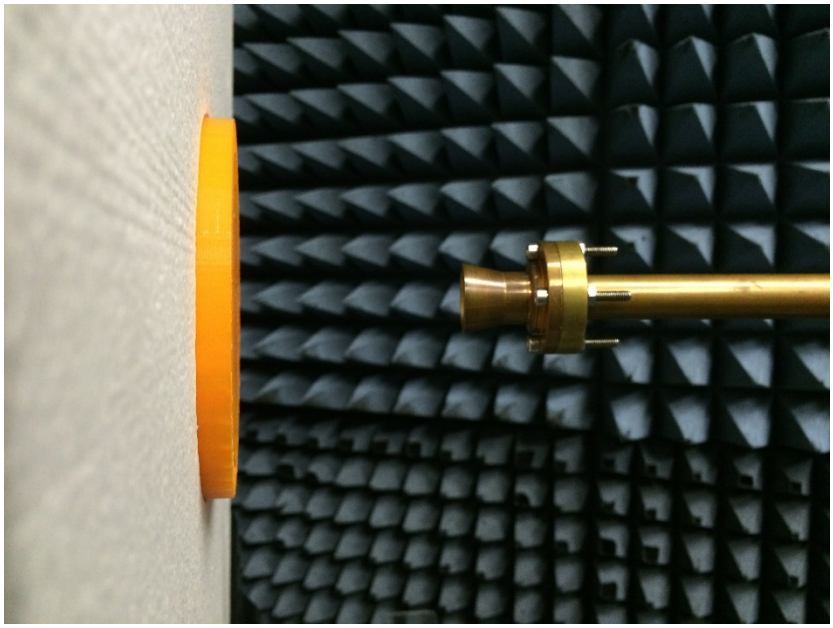

(a)

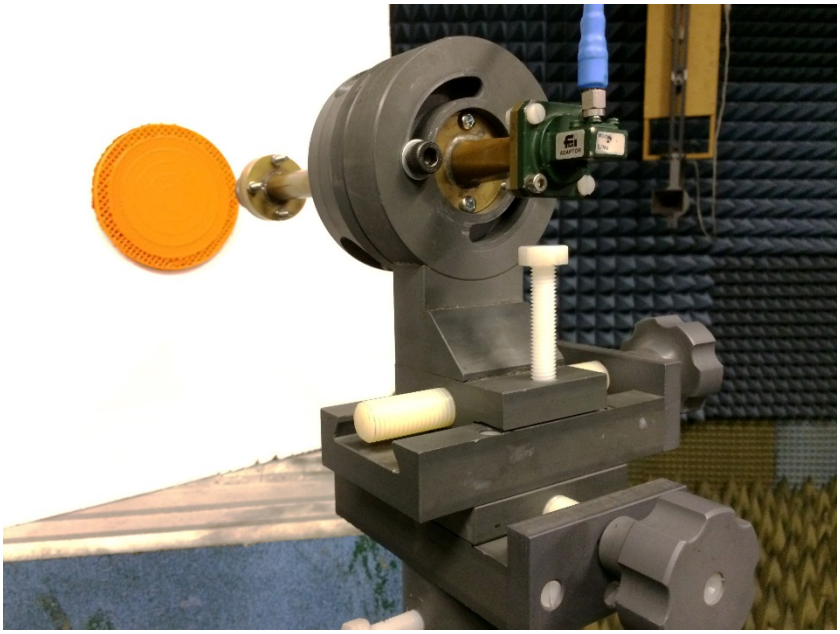

(b)

Fig. 7. *Measurement setup with the 3D-printed lens and fed by a conical horn at the focal point of the lens*

The first step was to place the feed horn on the lens axis with different feed distances to find the optimal focal point distance. The distance *z* indicated different distances between the feed horn and the lens surface and it was varied from 130 mm to 170 mm. Fig. 8 shows the measured broadband gain results of the lens antenna at boresight (theta = 0°), compared with the simulated gain with the feed horn placed 150 mm away. The gain of the 3D-printed lens antenna increased with frequency as was also found in the

simulation results. The highest gain was observed when the feed horn was placed 150 mm away from the lens surface which matched the designed focal distance. The lens antenna with far feeding (160 mm and 170 mm) had slightly higher gain compared with the close feeding (130 mm and 140 mm), particularly when the frequency was higher than 15 GHz. Moreover, 130 mm feeding had a lower gain compared with 140 mm feeding above 16.2 GHz. However, the measurement results indicated that the small amount of feed distance shifting had insignificant impact on this 3D-printed GRIN lens gain. The simulated gain varied from 18 to 24 dBi over the entire 12 to 18 GHz range, whilst the measured gain ranged from approximately 16 to 24 dBi. The conical horn had a gain from 7 to 13 dBi from 12 to 18 GHz; therefore, the lens provided a gain increase of 9 to 11 dB over the frequency of the Ku-band. The difference between simulated and measured gain values was due to the aberrations of the 3D-printed lens. The aberration was mainly due to fabrication tolerance of the infill density which was limited by the resolution of the printer. The interfaces between adjacent rings could also introduce differences between simulated and measured results.

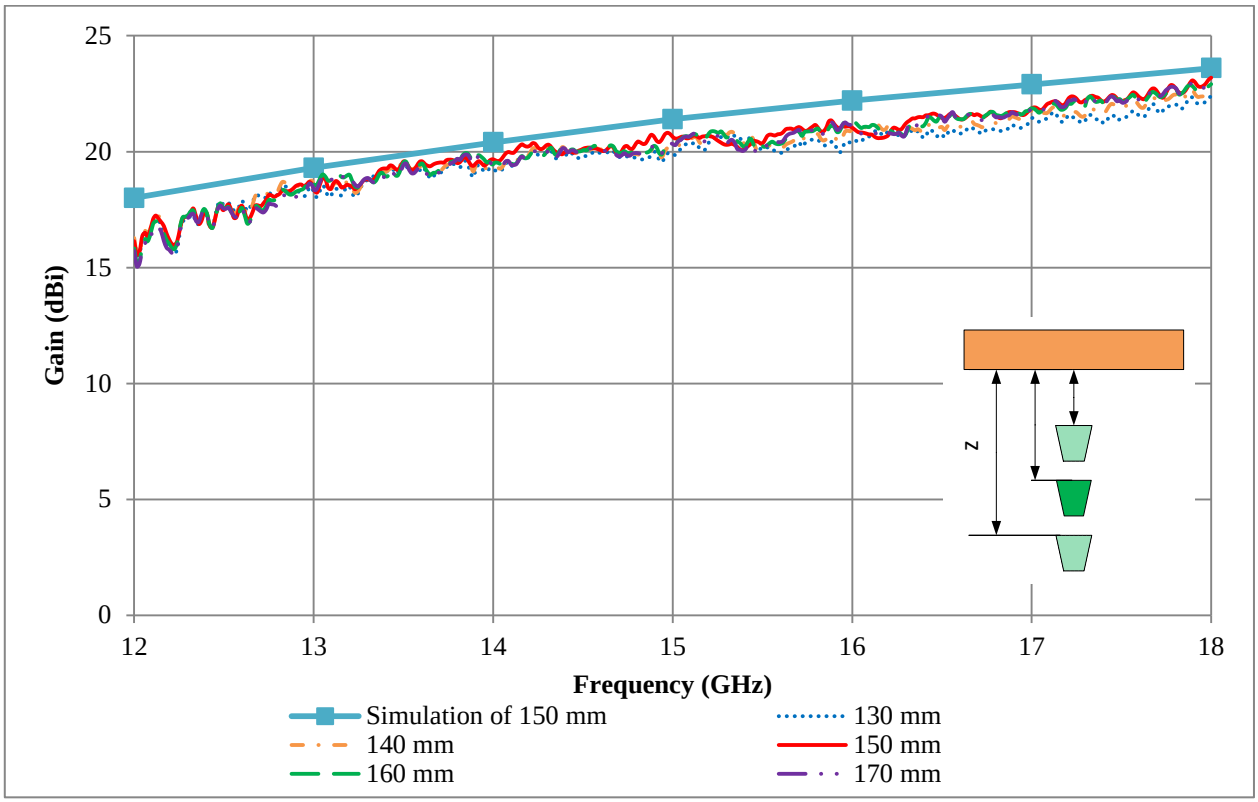

Fig. 8. *Measured broadband gain of 3D-printed lens with different feeding distances*

The measured gain patterns in the E-plane and H-plane of the lens, at the frequency of 12, 15 and 18 GHz, are shown in Fig. 9, and good agreement is seen with the simulated patterns in Fig. 4. The radiation patterns had a higher directive main beam at higher frequencies. The secondary side-lobes were due to the feed source. At 15 GHz the half-power beamwidth in the H-plane was approximately 11° and 9.5° at 18 GHz. The peak of the main beam was approximately 13.8 dB higher than the first side lobe level at the centre frequency 15 GHz.

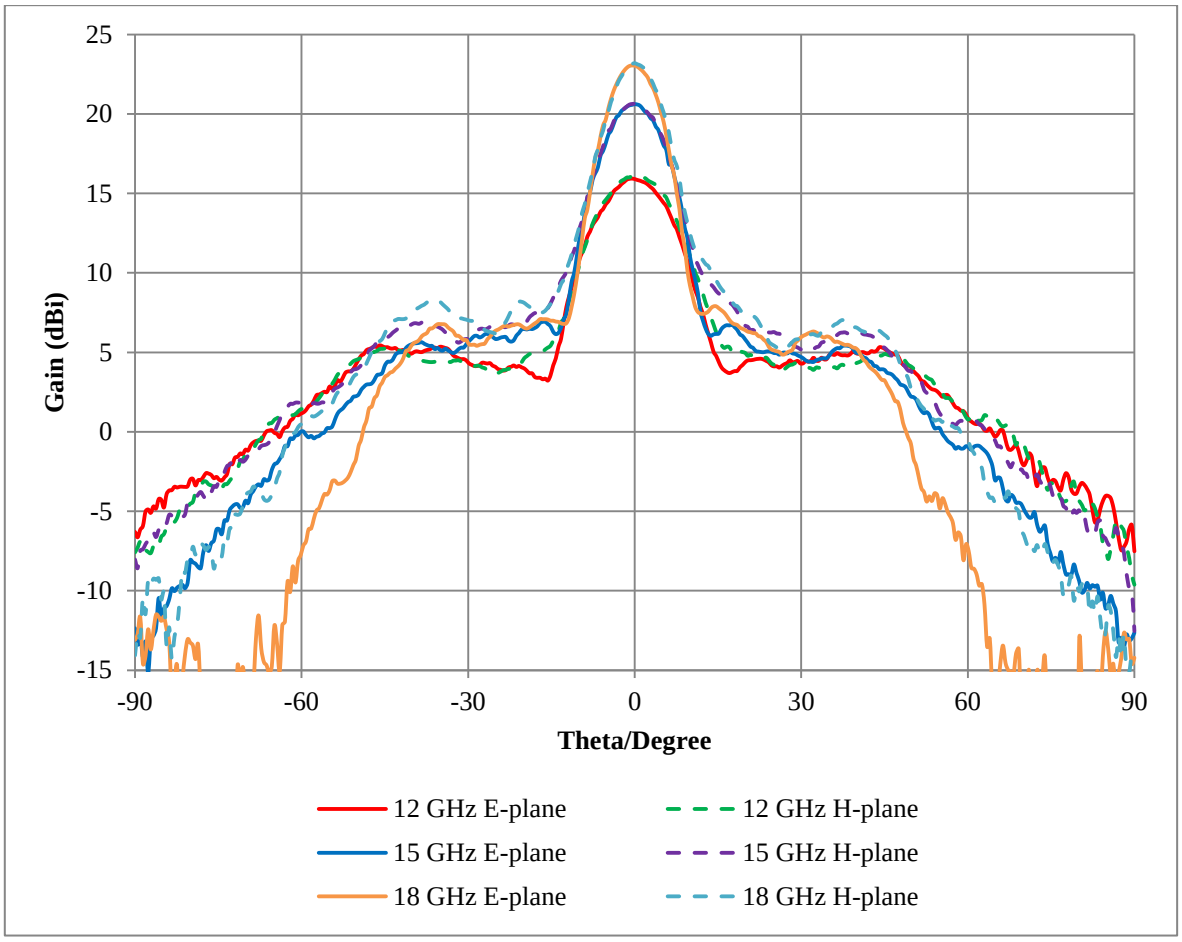

***Fig. 9**. Measured far-field pattern of 3D-printed lens antenna*

Moving the feed horn off the lens axis resulted in shifting the main beam and increasing the side-lobe levels. Fig. 10 shows the results of the off-axis experiment at 15 GHz. The feed horn was moved by a distance *x* in the azimuth-plane. When the feed horn was moved one wavelength (20 mm at 15 GHz) away from the lens axis, an 8° main lobe shifting was observed on the opposite side of the axis. The side-lobe level increased by approximately 1.5 dB at the same side of the feed horn and reduced by the same amount on the other side of the axis. The main beam was moved to 11.5° off-axis after the feed horn was moved 3

cm away from the lens axis. The side-lobe level was increased by 0.8 dB at the feed horn side. Therefore, illuminating the lens with multiple feeds around the lens axis could realise greater beam scanning coverage.

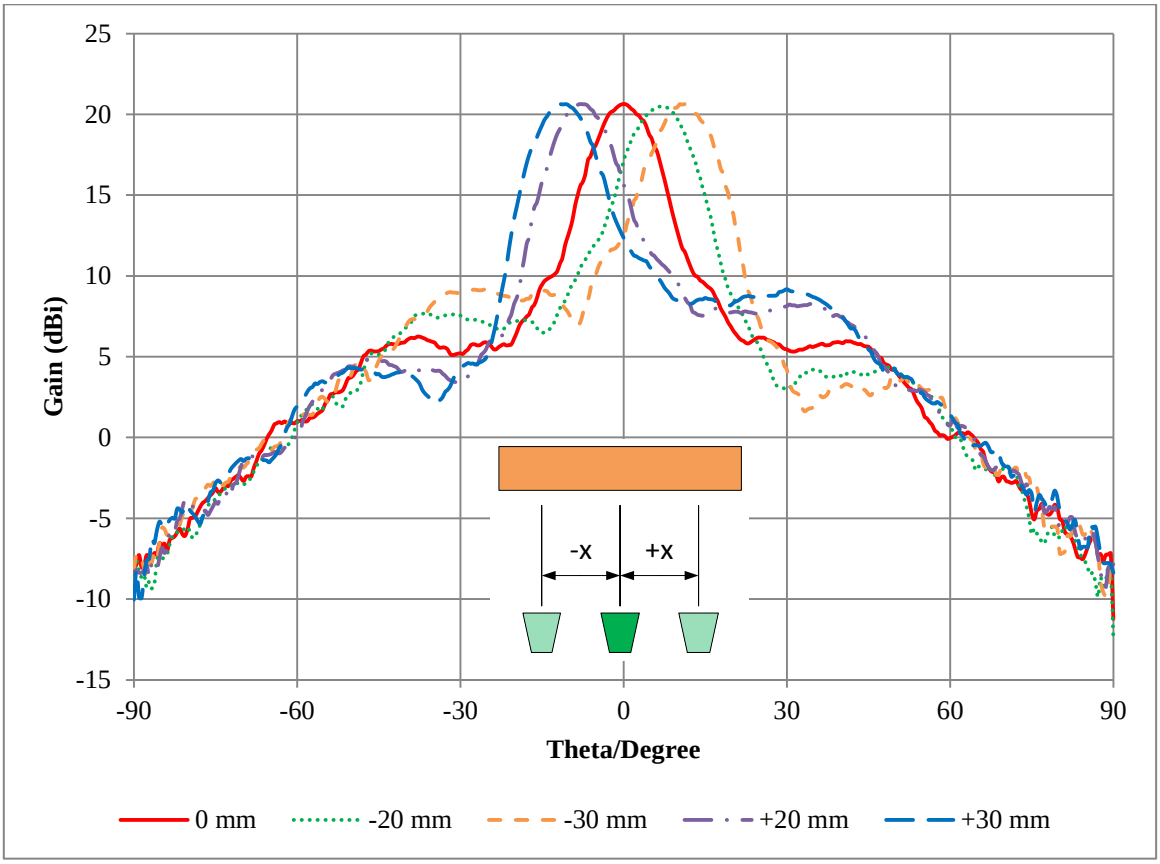

Fig. 10. *Measured patterns of 3D-printed lens with the horn positioned at different off axis distances at 15 GHz*

5. DaD Lens Design

Next, to decrease the profile of the earlier 3D-printed lens, we decrease the thickness of the lens by a factor of 2, so that the thin lens has a thickness of 9 mm instead of 18.5 mm. We also keep the same focal length (F) for this lens. Decreasing the thickness will force us to increase the dielectric permittivity by four times to maintain the same phase difference through the lens. By doing so, new design will have ring dielectric values as in Table 3. We see that these permittivity values are relatively high; furthermore, we note that the COTS materials with these permittivity values are not readily available.

Table 3 Design parameters for thin uniform lens with higher permittivities

ε_{r1}	ε_{r2}	ε_{r3}	ε_{r4}	ε_{r5}	ε_{r6}
10.88	10.40	9.52	8.32	6.84	5.20

We employ a unique technique for engineering artificial materials to achieve the dielectric parameters we need to implement our design by employing the technique of Dial-a-Dielectric (DaD) [3]. In this method we tweak the material by placing metallic patches in the middle of the dielectric rings, as shown in Fig. 11. The novelty of this method is that this method does not depend on resonance properties of patches to realize the permittivity and hence it does not suffer from the issues of bandwidth and losses. The key concept behind the low-loss design is that the patch dimensions are relatively small, as the patches are used in conjunction with available materials to achieve the desired transmission phase.

While we are able to create the dielectric materials shown in Table 3 by using the DaD techinque, but to keep the reflections low from the lens, we uniformly decrease the permittivity values of all the rings while maintaining the same phase difference through the dielectric rings. This strategy helps reduce the permittivity values as is evident from Table 4.

Table 4 Design parameters for thin uniform lens

ε_{r1}	ε_{r2}	ε_{r3}	ε_{r4}	ε_{r5}	ε_{r6}
4.95	4.59	3.98	3.16	2.22	1.30

We see in Table 4 that this thin lens needs higher permittivity values for ring 1-4 and lower values for rings 5-6 than those provided by the PLA ($\varepsilon_r = 2.72$). Thus, we use the DaD technique for rings 1-4 and uniform dielectrics for rings 5-6 which can be designed by PLA infill method as explained earlier. We refer new lens as the DaD lens (see Fig. 11) which requires material parameters listed in Table 5. This table also lists the size of the patches needed for the respective rings. This design has favourable advantage that we can use the same base material (here, PLA) for the 3D-printing.

Table 5 Design parameters for DaD lens

Ring No.	ε_{r1}	*a (mm)*
1	2.72	0.824
2	2.72	0.790

3	2.72	0.712
4	2.72	0.502
5	2.22	N/A
6	1.30	N/A

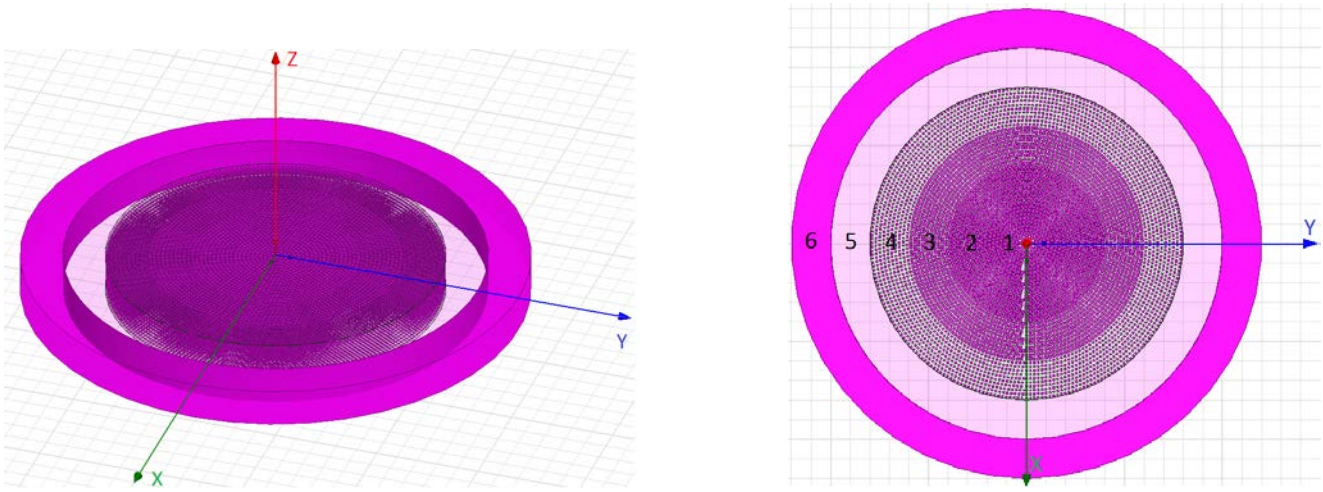

(a) (b)

Fig. 11. *DaD Lens; (a) Isometric view and (b) Top view*

To tweak the COTS materials, we use square patches, distributed in a circular pattern as shown in Fig. 11, and print them in the middle of the dielectric rings to realize the desired ε_r values. Unlike the previously published synthesis techniques, the present approach does not rely on resonance properties of patches or aperture to realize the artificial dielectrics; hence it circumvents the problem of losses and narrow bandwidths suffered by metamaterials.

Each dielectric ring is 10mm wide. Each patch-dielectric block is of size 1 mm × 1 mm × 1 mm so each dielectric ring can contain 10 such patch-dielectric blocks radially. The height of dielectric ring is 9 mm. Therefore, we place 9 such patch-dielectric blocks above each other to replace 9mm thick uniform dielectric. All patches are placed radially in such a fashion that they maintain an approximate periodicity of 1 mm × 1 mm as explained in [3].

In Fig. 12, we show the gain behaviour of lenses simulated by using Table 2, 4 and 5 for the thick lens, the thin uniform lens and the DaD lens, respectively. We do observe that DaD lens shows broadband behaviour and gain increases with frequency as expected. It is worthwhile to point out that gain results at Fig. 12 are different from those shown in Fig. 8, since the latter includes the gain of the feed horn, adding which makes the gain values comparable.

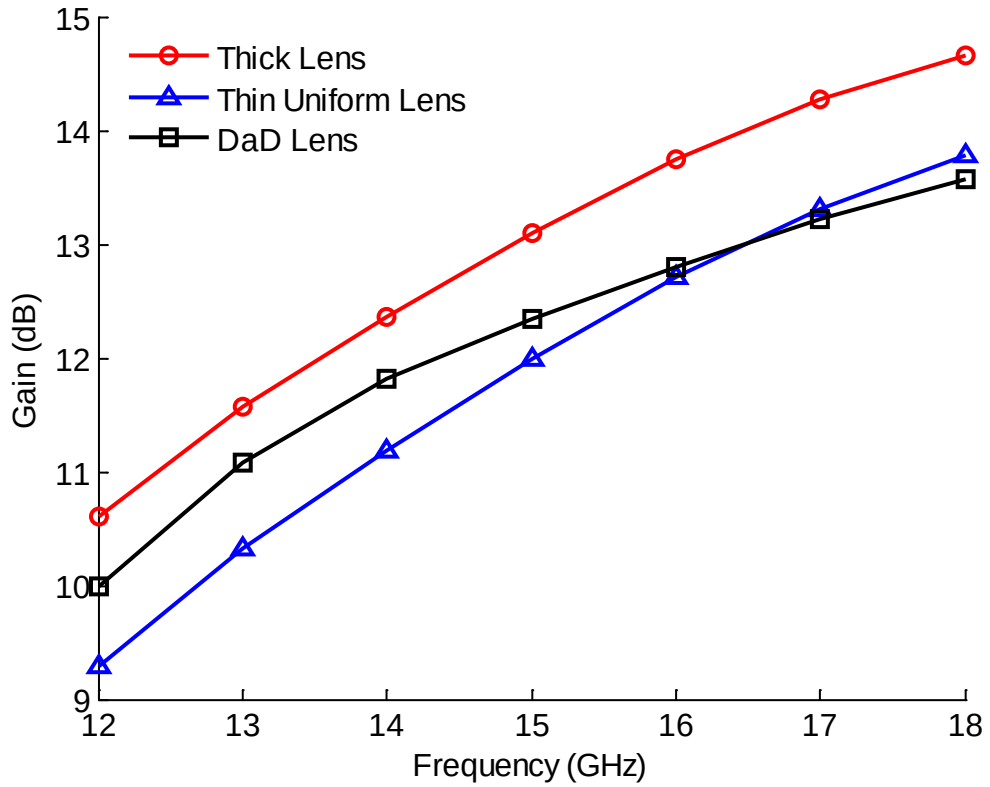

Fig. 12. *Simulated Gain Results*

6. Conclusions

This paper has presented low-cost, light-weight and wideband 3D-printed flat lenses which can be rapidly prototyped and be used for antenna applications. The entire thick lens was fabricated in one single process without the need for machining or manual assembly. The total print-time was approximately 4 hours and 20 minutes. The lens weighed approximately 130 g and the material cost was less than £7. The 12 cm diameter lens comprised of six concentric cylindrical rings with tailored permittivity values that were fabricated by varying the air/PLA volume fraction. The design equations for tailoring the effective permittivities using 3D-printing have been derived, and the measurement results of the lens showed that the equations were effective tools to estimate the required infill percentages. The lens had a broadband realised gain of 9 to 11 dBi from 12 to 18 GHz when illuminated by a conical horn. The lens was designed by using ray optics to have a 150 mm focal length; however, measurements as well as simulation results indicated that this distance was not very critical. In addition, moving the feed horn off the lens axis shifted the principal lobe that enables the future possibility of beam-scanning. The gain of the antenna could be further enhanced by increasing the number of concentric rings and thus obtaining a smoother permittivity gradient across the lens, or by adding matching layers to reduce the reflections but at the cost of increasing

the lens thickness. We have also presented a DaD lens that has a smaller thickness but with a gain value which is comparable to that of the thick 3D-printed flat lens.

7. Acknowledgments

This work was supported by EPSRC Doctoral Prize Research Fellowship.

8. References

[1] G. Savini, P. A. R. Ade, and J. Zhang, "A new artificial material approach for flat THz frequency lenses.," *Optics express*, vol. 20, no. 23, pp. 25766–25773, Nov. 2012.

[2] S. Jain, M. Abdel-Mageed, and R. Mittra, "Flat-lens design using field transformation and its comparison with those based on transformation optics and ray optics," *IEEE Antennas and Wireless Propagation Letters*, vol. 12, pp. 777–780, 2013.

[3] R. K. Arya, S. Pandey, R. Mittra, "Flat lens design using artificially engineered materials,' *Progress In Electromagnetics Research C*, Vol. 64, pp. 71–78, 2016.

[4] R. Yang, W. Tang, and Y. Hao, "A broadband zone plate lens from transformation optics.," *Optics express*, vol. 19, no. 13, pp. 12348–12355, 2011.

[5] O. Quevedo-Teruel, W. Tang, R. C. Mitchell-Thomas, A. Dyke, H. Dyke, L. Zhang, S. Haq, and Y. Hao, "Transformation optics for antennas: why limit the bandwidth with metamaterials?," *Scientific reports*, vol. 3, p. 1903, 2013.

[6] C. Mateo-Segura, A. Dyke, H. Dyke, S. Haq, and Y. Hao, "Flat Luneburg Lens via Transformation Optics for Directive Antenna Applications," *IEEE Transactions on Antennas and Propagation*, vol. 62, no. 4, pp. 1945–1953, 2014.

[7] Y. Zhang, R. Mittra, and W. Hong, "A zoned two-layer flat lens design," in *Final Program and Book of Abstracts - iWAT 2011: 2011 IEEE International Workshop on Antenna Technology: Small Antennas, Novel Structures and Innovative Metamaterials*, 2011, pp. 412–415.

[8] C. G. M. Ryan, M. R. Chaharmir, J. Shaker, J. R. Bray, Y. M. M. Antar, and a. Ittipiboon, "A wideband transmitarray using dual-resonant double square rings," *IEEE Transactions on Antennas and Propagation*, vol. 58, no. 5, pp. 1486–1493, 2010.

[9] A. Petosa and A. Ittipiboon, "Design and performance of a perforated dielectric Fresnel lens," *IEE Proceedings - Microwaves, Antennas and Propagation*, vol. 150, no. 5, p. 309, 2003.

[10] Y. Zhang, R. Mittra, and W. Hong, "On the Synthesis of a Flat Lens using a Wideband Low-Reflection Gradient-Index Metamaterial," *Journal of Electromagnetic Waves and Applications*, vol. 25, no. 16, pp. 2178–2187, 2011.

[11] C. C. Njoku, W. G. Whittow, and J. C. Vardaxoglou, "Simulation Methodology for Synthesis of Antenna Substrates With Microscale Inclusions," *IEEE Transactions on Antennas and Propagation*, vol. 60, no. 5, pp. 2194–2202, May 2012.

[12] Y. Zhang, R. Mittra, and W. Hong, "Systematic design of planar lenses using artificial dielectrics," in *2010 IEEE International Symposium on Antennas and Propagation and CNC-USNC/URSI Radio Science Meeting - Leading the Wave, AP-S/URSI 2010*, 2010.

[13] X. Chen, H. Feng Ma, X. Ying Zou, W. Xiang Jiang, and T. Jun Cui, "Three-dimensional broadband and high-directivity lens antenna made of metamaterials," *Journal of Applied Physics*, vol. 110, no. 4, 2011.

[14] C. C. Njoku, W. G. Whittow, and J. C. Vardaxoglou, "Comparative study of nanomaterials' effective

properties using canonical formations," in *Antennas and Propagation Conference (LAPC), 2010 Loughborough*, 2010.

[15] C. L. Holloway, E. F. Kuester, J. Baker-Jarvis, and P. Kabos, "A double negative (DNG) composite medium composed of magnetodielectric spherical particles embedded in a matrix," *IEEE Transactions on Antennas and Propagation*, vol. 51, no. 10, pp. 2596–2603, Oct. 2003.

[16] X. Cai, R. Zhu, and G. Hu, "Experimental study for metamaterials based on dielectric resonators and wire frame," *Metamaterials*, vol. 2, no. 4, pp. 220–226, Dec. 2008.

[17] D. R. Smith, J. J. Mock, A. F. Starr, and D. Schurig, "Gradient index metamaterials," *Physical Review E*, vol. 71, no. 3, p. 036609, Mar. 2005.

[18] T. Driscoll, D. N. Basov, A. F. Starr, P. M. Rye, S. Nemat-Nasser, D. Schurig, and D. R. Smith, "Free-space microwave focusing by a negative-index gradient lens," *Applied Physics Letters*, vol. 88, no. 8, p. 081101, 2006.

[19] H. F. Ma, B. G. Cai, T. X. Zhang, Y. Yang, W. X. Jiang, and T. J. Cui, "Three-dimensional gradient-index materials and their applications in microwave lens antennas," *IEEE Transactions on Antennas and Propagation*, vol. 61, no. 5, pp. 2561–2569, 2013.

[20] W. X. Jiang, T. J. Cui, H. F. Ma, X. M. Yang, and Q. Cheng, "Layered high-gain lens antennas via discrete optical transformation," *Applied Physics Letters*, vol. 93, no. 22, p. 221906, 2008.

[21] S. Zhang, C. C. Njoku, W. G. Whittow, and J. C. Vardaxoglou, "Novel 3D printed synthetic dielectric substrates," *Microwave and Optical Technology Letters*, vol. 57, no. 10, pp. 2344–2346, Oct. 2015.

[22] W. B. Weir, "Automatic measurement of complex dielectric constant and permeability at microwave frequencies," *Proceedings of the IEEE*, vol. 62, no. 1, pp. 33–36, 1974.

[23] K. S. Kelleher and C. Goatley, "Dielectric Lens for Microwaves," *Electronics*, pp. 142–145, 1955.

[24] C. A. Balanis, *Advanced Engineering Electromagnetics*. New York: Wiley, 2012.